

# Coloring Tetrahedral Semiconductors: Synthesis and Photoluminescence Enhancement of Ternary $\text{II-III}_2\text{-VI}_4$ Colloidal Nanocrystals

Md Riad Sarkar Pavel, Yunhua Chen, Anuluxan Santhiran, Eunbyeol Gi, Kerly Ochoa-Romero, Gordon J. Miller, Gonzalo Guirado, Aaron J. Rossini, and Javier Vela\*



Cite This: *ACS Energy Lett.* 2024, 9, 5012–5018



Read Online

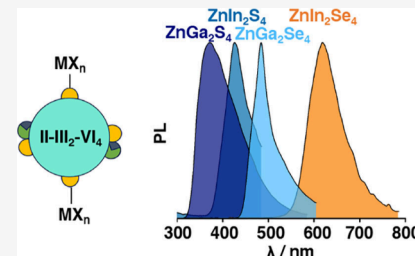
ACCESS |

Metrics & More

Article Recommendations

Supporting Information

**ABSTRACT:** Ternary tetrahedral  $\text{II-III}_2\text{-VI}_4$  semiconductors, where II is Zn or Cd, III In or Ga, and VI S, Se, or Te, are of interest in UV radiation detectors in medicine and space physics as well as  $\text{CO}_2$  photoreduction under visible light. We synthesize colloidal  $\text{II-III}_2\text{-VI}_4$  semiconductor nanocrystals from readily available precursors and ascertain their ternary nature by structural and spectroscopic methods, including  $^{77}\text{Se}$  solid-state NMR spectroscopy. The pyramidal shaped nanocrystals range between 2 and 12 nm and exhibit optical gaps of 2–3.9 eV. In the presence of excess anions on the particle surface, treatment with Lewis acidic, Z-type ligands results in better passivation and enhanced photoluminescence. Electronic structure calculations reveal the most stable, lowest energy polymorphs and coloring patterns. This work will pave the way toward more environmentally friendly, ternary semiconductors for optoelectronics and electrocatalysis.



Tetrahedral semiconductors are indispensable materials in both established and emerging technologies ranging from advanced computing and telecommunications to biophotonics and renewable energy.<sup>1–3</sup> For example, doped diamond finds use in various electrochemical sensors and high-power electronics, whereas silicon plays a crucial role in transistors, computer chips, and solar cells.<sup>4,5</sup> CdTe, GaN, GaAs, and other tetrahedral binary semiconductors are useful in lasers, solar cells, detectors, nanoinks, tunneling diodes, and imaging applications.<sup>6,7</sup> At the nanoscale, the chemistry of unary (elemental) and binary tetrahedral semiconductors continues to advance at a rapid pace.<sup>8</sup> Doped systems and solid solutions such as  $\text{In}_x\text{Ga}_{1-x}\text{As}$ ,  $\text{Hg}_{1-x}\text{Cd}_x\text{Te}$ , and atomically precise ternaries such as  $\text{CuInS}_2$  are of growing interest because of their infrared activity.<sup>9–11</sup> Other tetrahedral ternary semiconductors with band gaps in the visible region provide additional opportunities for fundamental research and technological development.<sup>12,13</sup>

Ternary tetrahedral semiconductors with the general formula  $\text{II-III}_2\text{-VI}_4$ , where II is Zn or Cd, III a group 13 element (“triel” or Tr) like In or Ga, and VI a chalcogen (Ch) such as S, Se, or Te, have rich crystallography and a wide array of optoelectronic properties (Figure 1a). With band gaps in the ~2–4 eV range,  $\text{II-III}_2\text{-VI}_4$  semiconductors exhibit birefringence, nonlinear susceptibility, and intense photoluminescence.<sup>14,15</sup> Their photosensitivity makes them useful in UV

radiation detectors for medicine and space physics.<sup>16</sup>  $\text{ZnGa}_2\text{Se}_4$ ,  $\text{ZnGa}_2\text{Te}_4$ , and  $\text{CdGa}_2\text{Te}_4$  could also be efficient catalysts.<sup>17,18</sup> A computational screening based on optical cross sections ( $\epsilon > 3.6 \times 10^4 \text{ cm}^{-1} \text{ eV}$ ), exciton binding energies (<200 meV), and absorption anisotropies (>0.8) predicted  $\text{CO}_2$  activity comparable to that of anatase  $\text{TiO}_2$ , but under visible light.<sup>17</sup> Some  $\text{II-III}_2\text{-VI}_4$  compositions are less toxic alternatives to more commonly used semiconductors.

Built from corner sharing  $[\text{IICh}_4]^{6-}$  and  $[\text{TrCh}_4]^{5-}$  tetrahedra,  $\text{II-III}_2\text{-VI}_4$  semiconductors adopt a chalcopyrite-type structure with an ordered cation vacancy arrangement.<sup>19</sup> Among multiple polymorphs, space groups  $\bar{I}42d$  and  $F\bar{4}3m$  prevail at higher temperatures.<sup>20</sup>  $\text{ZnGa}_2\text{S}_4$  crystallizes in three tetragonal polymorphs ( $\bar{I}42m$ ,  $P\bar{4}2m$ , and  $\bar{I}\bar{4}$ ),<sup>21</sup> whereas  $\text{ZnGa}_2\text{Se}_4$  has one cubic ( $F\bar{4}3m$ ) and two tetragonal structures ( $\bar{I}42m$  and  $\bar{I}\bar{4}$ ), see below and Supporting Information (SI).  $\text{ZnIn}_2\text{S}_4$  has one cubic ( $Fd\bar{3}mS$ ), two trigonal ( $P\bar{3}m1$ ,  $R3mH$ ),

Received: July 26, 2024

Revised: August 28, 2024

Accepted: August 29, 2024

Published: September 20, 2024



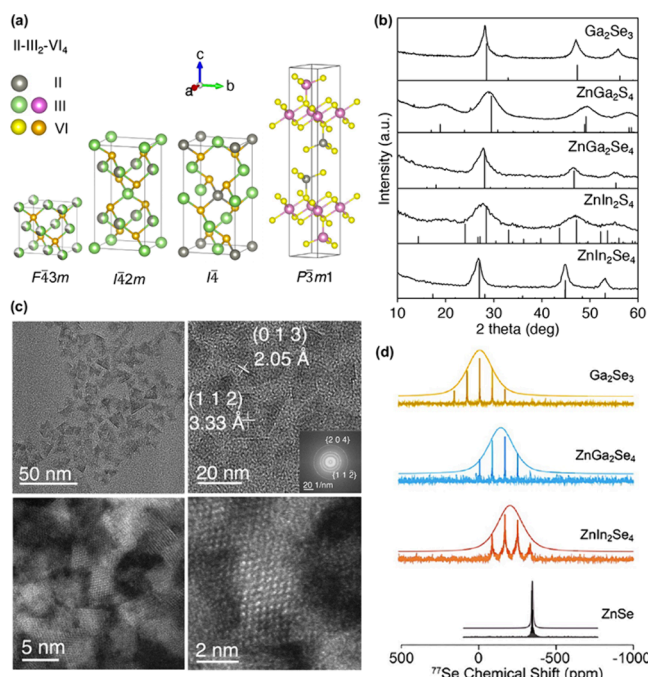


**Figure 1.** (a) Unit cells of select II-III<sub>2</sub>-VI<sub>4</sub> polymorphs. (b) Powder XRD of ZnGa<sub>2</sub>S<sub>4</sub>, ZnGa<sub>2</sub>Se<sub>4</sub>, ZnIn<sub>2</sub>S<sub>4</sub>, ZnIn<sub>2</sub>Se<sub>4</sub>, and Ga<sub>2</sub>Se<sub>3</sub> nanocrystals and standards (ICSD-44886, ICSD-44887, ICSD-15637, ICSD-25647, and ICSD-76754, respectively). (c) Representative bright-field, fast Fourier transform (FFT), and dark-field TEM of 8.2 ± 3.8 nm ZnIn<sub>2</sub>Se<sub>4</sub>. (d) Experimentally measured direct excitation <sup>77</sup>Se CPMG SSNMR spectra of Ga<sub>2</sub>Se<sub>3</sub>, ZnGa<sub>2</sub>Se<sub>4</sub>, and ZnIn<sub>2</sub>Se<sub>4</sub> nanocrystals, acquired with a MAS frequency of 25 kHz, a CPMG pulse sequence, 75 s recycle delay, and averaging 1024 scans; 9.4 T magnetic field. Peak fits overlaid on experimental CPMG NMR.

and one hexagonal polymorph ( $P6_3mc$ ), whereas ZnIn<sub>2</sub>Se<sub>4</sub> has three with mixed-Zn/Ga cation sites.

High temperature solid-state reactions using the elements,<sup>22,23</sup> or between the lower order binaries,<sup>24</sup> result in poly- (bulk) or single-crystal versions of II-III<sub>2</sub>-VI<sub>4</sub> materials. Molecular beam epitaxy and chemical bath deposition produce thin films of ZnGa<sub>2</sub>Se<sub>4</sub> and ZnIn<sub>2</sub>Se<sub>4</sub>.<sup>25</sup> Solvothermal methods generate ZnIn<sub>2</sub>S<sub>4</sub> microspheres,<sup>26,27</sup> as well as II/III/VI frameworks that resemble Sn- and S-doped versions of ZnGa<sub>2</sub>Se<sub>4</sub>.<sup>28</sup> A few syntheses<sup>29–31</sup> generate nanoscale versions of ZnGa<sub>2</sub>S<sub>4</sub>, ZnGa<sub>2</sub>Se<sub>4</sub>, and ZnIn<sub>2</sub>S<sub>4</sub>. Colloidal II-III<sub>2</sub>-VI<sub>4</sub> nanocrystals remain underexplored.

Here we present a widely applicable and reproducible route to prepare ternary II-III<sub>2</sub>-VI<sub>4</sub> nanocrystals. This method generates stable colloidal solutions of monodisperse (2–12 nm) particles of ZnGa<sub>2</sub>S<sub>4</sub>, ZnGa<sub>2</sub>Se<sub>4</sub>, ZnIn<sub>2</sub>S<sub>4</sub>, and ZnIn<sub>2</sub>Se<sub>4</sub> from commercially available precursors. We characterize the nanocrystals using X-ray diffraction, UV-visible absorption, photoluminescence (PL), electrochemistry, and solid-state NMR spectroscopy. While routine powder XRD fails to distinguish their binary impurities, SSNMR confirms the identity and purity of the ternary II-III<sub>2</sub>-VI<sub>4</sub> nanophases. The photoluminescence of the nanocrystals can be enhanced by treatment with Lewis acids (Z-type ligands). Electronic structure calculations unveil the relative energies of their different polymorphs and coloring patterns.

Injection of bis(trimethylsilyl)sulfide (TMS<sub>2</sub>S) or diphenyl diselenide (PhSeSePh) into a mixture of Zn(OAc)<sub>2</sub>·2H<sub>2</sub>O and

### Scheme 1. Solution-Phase Synthesis and Metal-Halide Treatment of Colloidal II-III<sub>2</sub>-VI<sub>4</sub> and III<sub>2</sub>VI<sub>3</sub> Nanocrystals.

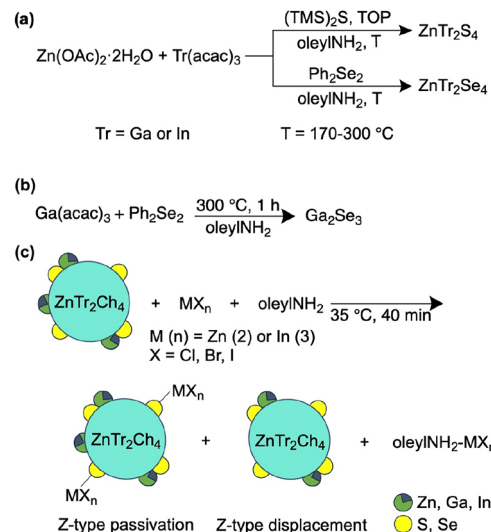


**Table 1. Synthesis of Colloidal II-III<sub>2</sub>-VI<sub>4</sub> Nanocrystals<sup>a</sup>**

precursors <sup>a</sup>			<i>T</i> (°C)	product(s) (Scherrer, TEM/nm)
Zn(II) 0.1 mM	Tr(III) 0.2 mM	Ch(VI) 0.4 mM		
OAc	Ga(acac) <sub>3</sub>	(TMS) <sub>2</sub> S	300	ZnGa <sub>2</sub> S <sub>4</sub> (2.3 ± 0.1)
OAc	Ga(acac) <sub>3</sub>	Ph <sub>2</sub> Se <sub>2</sub>	290	ZnGa <sub>2</sub> Se <sub>4</sub> (4.7 ± 0.4)
OAc	In(acac) <sub>3</sub>	(TMS) <sub>2</sub> S	170	ZnIn <sub>2</sub> S <sub>4</sub> (3.3 ± 1.6)
OAc	In(acac) <sub>3</sub>	Ph <sub>2</sub> Se <sub>2</sub>	270	ZnIn <sub>2</sub> Se <sub>4</sub> (5.6 ± 0.1, 8.2 ± 3.8)
OAc	Ga(acac) <sub>3</sub>	Ph <sub>2</sub> Se <sub>2</sub>	300	Ga <sub>2</sub> Se <sub>3</sub> (6.7 ± 0.5)

<sup>a</sup>6 mL oleylNH<sub>2</sub> + TOP; 1 h; St = stearate.

Tr(acac)<sub>3</sub> (Tr = Ga, In) in oleylamine at 100 °C, followed by heating to 170–300 °C, results in colloidal II-III<sub>2</sub>-VI<sub>4</sub> nanocrystals (Scheme 1). Powder X-ray diffraction (XRD) of solids isolated from this reaction are consistent with the standard patterns reported for  $\bar{I}4$  ZnGa<sub>2</sub>S<sub>4</sub>,  $\bar{I}4$  ZnGa<sub>2</sub>Se<sub>4</sub>,  $P6_3mc$  ZnIn<sub>2</sub>S<sub>4</sub>, and  $\bar{I}4$  ZnIn<sub>2</sub>Se<sub>4</sub> (Figure 1b). Line width analysis reveals Scherrer dimensions between 2.3–5.6 nm (Table 1, see SI). Bright- and dark-field transmission electron microscopy (TEM) show uniform pyramidal morphologies. *d* Spacing from fast Fourier transform (FFT) measurements are consistent with the powder XRD data (Figure 1c). Energy dispersive X-ray spectroscopy (EDS) under the scanning electron microscope (SEM) yields the compositions: Zn<sub>0.8</sub>Ga<sub>2.0</sub>S<sub>4.7</sub>, Zn<sub>1.1</sub>Ga<sub>2.0</sub>Se<sub>2.7</sub>, Zn<sub>0.9</sub>In<sub>2.0</sub>S<sub>3.9</sub>, and Zn<sub>1.0</sub>In<sub>2.0</sub>Se<sub>3.9</sub>, in good agreement with the theoretical formulas. TEM-EDS analysis confirms all three elements are colocalized.

Unlike unary or binary nanocrystal synthesis, where precursor decomposition generates monomer units that coalesce into larger particles with the same composition as the final product, ternary (and other multinary) nanocrystal evolution involves multiple phases in a stepwise fashion:<sup>32,33</sup> For example, nucleation of Bi seeds precedes formation of colloidal NaBiS<sub>2</sub> and NaBiSe<sub>2</sub> nanocrystals.<sup>32</sup> Nucleation of metallic Zn seeds, followed by heterogeneous deposition of a Pn shell, precede formation of LiZnSb nanocrystals.<sup>34</sup> Successful synthesis of multinary colloids requires mild precursors and conditions capable of producing sufficiently small, reactive seeds that live long enough to proceed to these

additional heterogeneous nucleation, interfacial reaction, and phase transformation steps.

Reactions between long-chain zinc carboxylates, triel chlorides, and selenourea produce, instead of ternaries, mixtures of ZnSe and  $\text{SeO}_x$ . Unlike hydrolysis-prone triel chlorides, triel-acetylacetones are less reactive.<sup>35</sup> In addition, PhSeSePh contains a relatively weak Se–Se bond (43.63 kcal mol<sup>-1</sup>) and two stronger C(Ph)–Se bonds (64.4 kcal mol<sup>-1</sup>), both of which must break to release [Se].<sup>36–38</sup> We hypothesize that PhSe· radicals, generated by facile homolysis of the weaker Se–Se bond, suppress runaway growth of Zn-, Ga-, or In-based seeds. Interestingly, the metal–organic chalcogenolate  $\text{In}(\text{SePh})_3$  precedes ternary  $\text{ZnIn}_2\text{Se}_4$  (SI).<sup>39,40</sup> At higher temperatures ( $\geq 200^\circ\text{C}$ ), this intermediate then reacts with the [Se] released from *in situ* cleavage of the C–Se bonds in PhSeSePh to yield  $\text{ZnIn}_2\text{Se}_4$  nanocrystals (Table 1).<sup>36</sup>

In the case of the sulfur-derived nanocrystals, the metal acetate or oleylamine complex formed *in situ* may react with  $\text{TMS}_2\text{S}$  to form binary seeds ( $\text{ZnS}$ ,  $\text{Tr}_2\text{S}_3$ ),<sup>41</sup> which subsequently evolve into ternary nanocrystals. The synthesis of chalcopyrite nanocrystals follows a similar phase evolution.<sup>42</sup> While our approach provides a synthetic entry into phase-pure ternary nanocrystals, otherwise parasitic side reactions can be put to good use. For example, reaction between  $\text{Ga}(\text{acac})_3$  and  $\text{Ph}_2\text{Se}_2$  at  $300^\circ\text{C}$  produces freestanding, colloidal  $F43m$   $\text{Ga}_2\text{Se}_3$  nanocrystals. Only substrate-bound versions of these were reported.<sup>43,44</sup> Scherrer analysis of XRD peak widths yields an average size of  $6.7 \pm 0.5$  nm, with a slightly Se-rich EDX composition of  $\text{Ga}_{2.0}\text{Se}_{3.6}$ .

The standard XRD patterns of ternary II-III<sub>2</sub>-VI<sub>4</sub> and binary III<sub>2</sub>VI<sub>3</sub> materials are very similar (Figure 1b), making unambiguous confirmation of ternary composition difficult based on powder XRD alone. While EDX area scans and colocalization data above are consistent with a near-stoichiometric ternary composition, we sought an additional technique that would unequivocally probe the structure of the nanocrystals at the atomic level. Solid-state (SS)NMR spectroscopy measures the chemical shift of NMR active nuclei based on the local environment of the different chemical sites, thus enabling the determination of the true speciation of a sample.<sup>45</sup> Thus, we resorted to <sup>77</sup>Se SSNMR spectroscopy to conclusively ascertain the ternary structure and distinguish  $\text{ZnGa}_2\text{Se}_4$  and  $\text{ZnIn}_2\text{Se}_4$  from  $\text{Ga}_2\text{Se}_3$  and  $\text{ZnSe}$ .

The lowest energy polymorph of  $\text{ZnGa}_2\text{Se}_4$ , and  $\text{ZnIn}_2\text{Se}_4$ ,  $\overline{\text{I}4}$ , (see below) possesses one <sup>77</sup>Se coordination environment:  $\text{SeZnTr}_2$ . To enhance the sensitivity of <sup>77</sup>Se SSNMR experiments, we used a Carr–Purcell Meiboom–Gill (CPMG) pulse sequence.<sup>46–48</sup> Each of  $\text{ZnGa}_2\text{Se}_4$  and  $\text{ZnIn}_2\text{Se}_4$  exhibits unique, inhomogeneously broadened <sup>77</sup>Se peaks (Figure 1d), in agreement with other nanocrystals.<sup>49–51</sup> This broadening reflects the small particle size, which creates a distribution of surface, near-surface, and interior (bulk-like) Se sites. By coupling of spin  $1/2$  <sup>77</sup>Se nuclei to the abundant quadrupolar nuclei, <sup>69/71</sup>Ga or <sup>115</sup>In could also cause inhomogeneous broadening. Critically, <sup>77</sup>Se SSNMR spectra of binary  $\text{Ga}_2\text{Se}_3$  and  $\text{ZnSe}$  exhibit different chemical shifts. Crystalline  $\beta$ - $\text{Ga}_2\text{Se}_3$  features Se atoms that bind to two- or three-Ga atoms with approximate chemical shifts of 190 ppm and 0 ppm, respectively.<sup>52</sup> Because the distribution of <sup>77</sup>Se chemical shifts exceeds the chemical shift differences, we observe a single broad peak for  $\text{Ga}_2\text{Se}_3$ . The <sup>77</sup>Se SSNMR spectra of synthesized and commercial  $\text{ZnSe}$  are much narrower than those of  $\text{Ga}_2\text{Se}_3$  or ternary nanocrystals.

The light absorption onsets of ternary nanocrystals are between 2.0–3.9 eV (Figure 2a). This is consistent with band

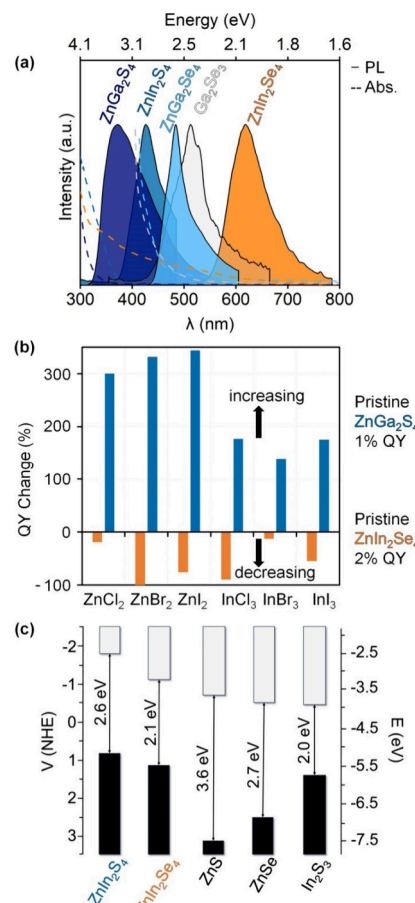


**Figure 2.** (a) Optical absorption and photoluminescence, (b) effect of Z-type (Lewis acidic) ligands on PL QY, and (c) electrochemically determined energies of II-III<sub>2</sub>-VI<sub>4</sub> nanocrystals (bulk  $\text{ZnS}$ ,  $\text{ZnSe}$ , and  $\text{In}_2\text{S}_3$  included for reference).

gap values derived from extrapolation of the linear region of direct  $(\text{Abs}\cdot h\nu)^2$  vs  $(h\nu)$  Tauc plots (Table 2 and SI). The

**Table 2. Band Gaps of II-III<sub>2</sub>-VI<sub>4</sub> and III<sub>2</sub>VI<sub>3</sub> Nanocrystals.**

composition	band gap energy (eV)				
	experimental		lit	theoretical	
	abs	echem		VASP	LMTO
$\text{ZnGa}_2\text{S}_4$	3.9	nd <sup>a</sup>	3.3	2.3	2.3
$\text{ZnGa}_2\text{Se}_4$	2.7	nd <sup>a</sup>	2.4	1.2	1.2
$\text{ZnIn}_2\text{S}_4$	3.2	2.6	2.3		
$\text{ZnIn}_2\text{Se}_4$	2.1	2.1	2.2		
$\text{Ga}_2\text{Se}_3$	2.0	nd <sup>a</sup>	2.1		
$\text{ZnSe}$	2.7	nd <sup>a</sup>	2.7	1.7	1.1

<sup>a</sup>Not determined.

values are in agreement with previous literature reports from single crystals and thin films.<sup>23–26</sup> The absorption onset and optical gap of  $\text{Ga}_2\text{Se}_3$  nanocrystals are also consistent with single crystals<sup>44</sup> and are distinct from its ternary counterpart,  $\text{ZnGa}_2\text{Se}_4$ . Among ternaries, there is an inverse relationship between band gap value and isotropic <sup>77</sup>Se chemical shift. The optical band gap widens with increasing electronegativity of the

trial or lattice parameter,  $a$  (SI). A similar relationship exists for I–III–Ch<sub>2</sub> materials.<sup>53</sup>

Cyclic voltammograms (CVs) on glassy carbon electrodes display well-defined first oxidation and reduction waves under an inert atmosphere corresponding to the anodic and cathodic peak potentials as well as the oxidation and reduction onsets (SI). Different scan rates result in the same electrochemical peaks. The electrochemically measured ionization potentials (IP) and electron affinities (EA) for ZnIn<sub>2</sub>S<sub>4</sub>, ZnIn<sub>2</sub>Se<sub>4</sub>, and select binaries corroborate the band gap values obtained from optical absorption (Figure 2c).

All ternary II–III<sub>2</sub>–VI<sub>4</sub> nanocrystals display band edge photoluminescence (PL), with quantum yields (QYs) between 0.1–2.2% (Figure 2a). Postsynthetic modification with X-, L-, or Z-type ligands can minimize surface defects by passivating undercoordinated atoms or dangling bonds,<sup>54–56</sup> which act as surface traps and lower QYs via nonradiative recombination.<sup>57,58</sup> Interestingly, the effect of this treatment is highly dependent on particle stoichiometry: MX<sub>2</sub> (Z-type) treatment (M = Zn, In; X = Cl, Br, I) of sulfur-rich Zn<sub>0.8</sub>Ga<sub>2.0</sub>S<sub>4.7</sub> leads to a two- to four-fold enhancement in PL QY (+140–340%, see SI), whereas that of selenium-poor Zn<sub>1.0</sub>In<sub>2.0</sub>Se<sub>3.9</sub> decreases it significantly (~20–100%, Figure 2b). We hypothesize that MX<sub>2</sub>-induced PL enhancement in II–III<sub>2</sub>–VI<sub>4</sub> nanocrystals with anion-rich surfaces is due to Z-type passivation, while reduced PL in those with anion-deficient surfaces is due to Z-type displacement of surface cations (Scheme 1c). Similar QY increases were observed for II–VI and III–V QDs.<sup>57</sup>

To gain deeper insight into precise structure and atom ordering, we conducted *ab initio* calculations on ZnGa<sub>2</sub>S<sub>4</sub> and ZnGa<sub>2</sub>Se<sub>4</sub>. Beyond electronic structures of II–III<sub>2</sub>–VI<sub>4</sub> materials,<sup>21,59</sup> a comprehensive study of mixed site occupancies, superstructures or “coloring” patterns, is lacking.<sup>32,60,61</sup> Because the  $\bar{I}42m$  polymorph of ZnGa<sub>2</sub>S<sub>4</sub> features mixed cation sites (Figure 1), we considered three possible superstructures:  $\bar{I}42m$  S1,  $\bar{I}42m$  S2,  $\bar{I}42m$  S3 (SI). We constructed three superstructures for each of the two ( $\bar{I}42m$  and  $F\bar{4}3m$ ), out of three, polymorphs of ZnGa<sub>2</sub>Se<sub>4</sub> with mixed cation sites. The XRD patterns of the supercells fail to distinguish the experimental patterns, thus we utilized the Vienna *ab initio* simulation package (VASP)<sup>62</sup> to calculate the relative energies. Using the Perdew–Burke–Ernzerhof (PBE) functional, we relaxed the cell parameters prior to computing relative energies. Our results suggest that  $\bar{I}4$  is the lowest energy polymorph for ZnGa<sub>2</sub>S<sub>4</sub> and ZnGa<sub>2</sub>Se<sub>4</sub>, while the cubic and  $I42m$  S1 phases remain close in energy (Figure 3). Other superstructures are ~2.8–3.2 eV/f.u. less stable, likely due to the presence of short Ch–Ch contacts, as compared to the sum of the van der Waals radii,<sup>63</sup> resulting in destabilizing lone-pair and electrostatic cation–cation repulsions.<sup>64</sup>

Band structure and density of states (DOS) calculations using the linear muffin-tin orbital (LMTO) model with the all-electron, quasi-relativistic tight-binding LMTO program and the Atomic Spheres Approximation<sup>65</sup> show the lowest energy ( $\bar{I}4$ ) polymorphs of ZnGa<sub>2</sub>S<sub>4</sub> and ZnGa<sub>2</sub>Se<sub>4</sub> have direct gaps, with values of 1.37 and 2.25 eV, respectively (Figure 3b,c, and SI). These underestimate the experimental values by ca. 30–40%, a common feature of LDA calculations (for example, II–III<sub>2</sub>VI<sub>4</sub><sup>21</sup> and I–V–VI<sub>2</sub>).<sup>32</sup> Similar band structure calculations on ZnSe were used to validate our results. While VASP is slightly better than LMTO, both underestimate the well-known “bulk” ZnSe band gap of 2.70 eV by a comparable amount (Figure 3d,e and Table 2). Thus, the experimental band gaps of the

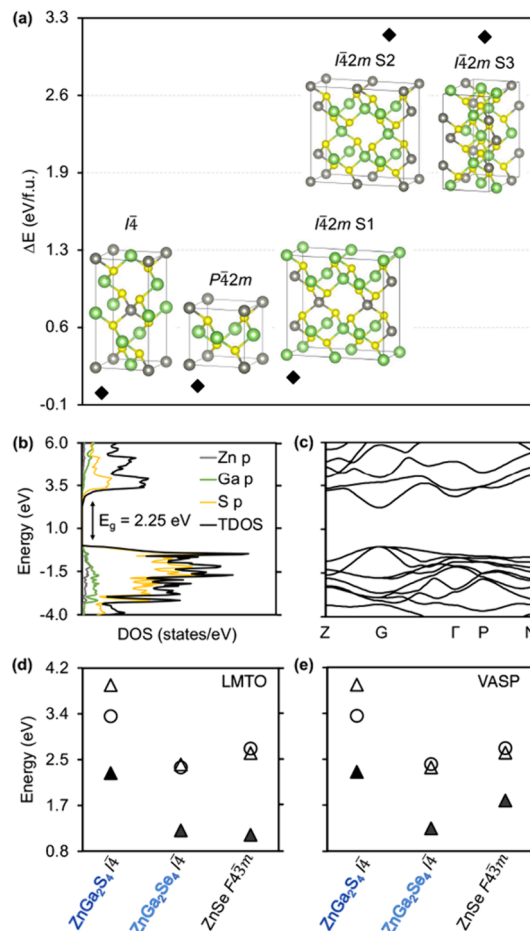


Figure 3. (a) Relative energies of ZnGa<sub>2</sub>S<sub>4</sub> polymorphs. (b) Density of states, and (c) band structure of  $\bar{I}4$  ZnGa<sub>2</sub>S<sub>4</sub>. Theoretical (▲), (d,e) experimental (△), and literature (○) band gaps of lowest energy tetragonal ( $\bar{I}4$ ) ZnGa<sub>2</sub>Se<sub>4</sub> and ZnGa<sub>2</sub>S<sub>4</sub> (zinc blende ZnSe added as reference).

ternary nanocrystals align best with those calculated for the  $\bar{I}4$  polymorphs.

In summary, we developed a highly reproducible colloidal synthesis of emissive ternary II–III<sub>2</sub>–VI<sub>4</sub> nanocrystals. A combination of structural, analytical, electrochemical, and spectroscopic methods, including <sup>77</sup>Se SSNMR, corroborates their ternary nature, homogeneity, and phase purity. Treatment with Lewis acidic Z-type ligands passivates chalcogen-rich nanocrystal surfaces, increasing the PL; in contrast, a similar treatment causes Z-type displacement of cations from anion-deficient surfaces, decreasing the PL. Electronic structure calculations identify lowest energy phases, shedding light on the experimental vs theoretical band gaps of II–III<sub>2</sub>–VI<sub>4</sub> materials. Future efforts will aim at testing the photo- and electrocatalytic activity of these materials.

## ASSOCIATED CONTENT

### Supporting Information

The Supporting Information is available free of charge at <https://pubs.acs.org/doi/10.1021/acsenergylett.4c02032>.

XRD, EM, QY, and SSNMR data, coloring and electronic structure calculations (PDF)

## AUTHOR INFORMATION

### Corresponding Author

Javier Vela — Department of Chemistry, Iowa State University, Ames, Iowa 50011, United States; Ames National Laboratory, Ames, Iowa 50011, United States;  orcid.org/0000-0001-5124-6893; Email: vela@iastate.edu

### Authors

Md Riad Sarkar Pavel — Department of Chemistry, Iowa State University, Ames, Iowa 50011, United States

Yunhua Chen — Department of Chemistry, Iowa State University, Ames, Iowa 50011, United States; Ames National Laboratory, Ames, Iowa 50011, United States

Anuluxan Santhiran — Department of Chemistry, Iowa State University, Ames, Iowa 50011, United States; Ames National Laboratory, Ames, Iowa 50011, United States

Eunbyeol Gi — Department of Chemistry, Iowa State University, Ames, Iowa 50011, United States; Ames National Laboratory, Ames, Iowa 50011, United States;  orcid.org/0000-0003-0846-8655

Kerly Ochoa-Romero — Departament de Química, Universitat Autònoma de Barcelona, 08193 Barcelona, Spain

Gordon J. Miller — Department of Chemistry, Iowa State University, Ames, Iowa 50011, United States;  orcid.org/0000-0001-5717-8000

Gonzalo Guirado — Departament de Química, Universitat Autònoma de Barcelona, 08193 Barcelona, Spain

Aaron J. Rossini — Department of Chemistry, Iowa State University, Ames, Iowa 50011, United States; Ames National Laboratory, Ames, Iowa 50011, United States;  orcid.org/0000-0002-1679-9203

Complete contact information is available at:

<https://pubs.acs.org/10.1021/acsenergylett.4c02032>

### Notes

The authors declare no competing financial interest.

## ACKNOWLEDGMENTS

We thank the U.S. National Science Foundation, Division of Chemistry, Macromolecular, Supramolecular, and Nanochemistry Program (2305062) for funding this work. G.G. and K.O.R. thank the European Union's Horizon Europe programme under the grant agreement no. 101115182 (CONFETI — HORIZON-EIC-2022-PATHFINDERCHALLENGES-01) for financial support. Y.C., A.S., and A.J.R. thank the U.S. Department of Energy (DOE), Materials Science and Engineering Division. Ames National Laboratory is operated for the U.S. DOE by Iowa State University, under contract no. DE-AC02-07CH11358. We thank Allie Roth and Marquix Adamson for assistance.

## REFERENCES

- (1) Li, Z.; Yan, T.; Fang, X. Low-dimensional Wide-bandgap Semiconductors for UV Photodetectors. *Nat. Rev. Mater.* **2023**, *8*, 587–603.
- (2) Kirmani, A. R.; Luther, J. M.; Abolhasani, M.; Amassian, A. Colloidal Quantum Dot Photovoltaics: Current Progress and Path to Gigawatt Scale Enabled by Smart Manufacturing. *ACS Energy Lett.* **2020**, *5*, 3069–3100.
- (3) Ahn, N.; Livache, C.; Pinchetti, V.; Klimov, V. I. Colloidal Semiconductor Nanocrystal Lasers and Laser Diodes. *Chem. Rev.* **2023**, *123*, 8251–8296.
- (4) Lin, H.; Yang, M.; Ru, X.; Wang, G.; Yin, S.; Peng, F.; Hong, C.; Qu, M.; Lu, J.; Fang, L.; Han, C.; Procel, P.; Isabella, O.; Gao, P.; Li, Z.; Xu, X. Silicon Heterojunction Solar Cells with up to 26.81% Efficiency Achieved by Electrically Optimized Nanocrystalline-Silicon Hole Contact Layers. *Nat. Energy* **2023**, *8*, 789–799.
- (5) Huo, H.; Janek, J. Silicon as Emerging Anode in Solid-State Batteries. *ACS Energy Lett.* **2022**, *7*, 4005–4016.
- (6) Wu, Z.; Liu, P.; Zhang, W.; Wang, K.; Sun, X. W. Development of InP Quantum Dot-Based Light-Emitting Diodes. *ACS Energy Lett.* **2020**, *5*, 1095–1106.
- (7) García de Arquer, F. P.; Talapin, D. V.; Klimov, V. I.; Arakawa, Y.; Bayer, M.; Sargent, E. H. Semiconductor Quantum Dots: Technological Progress and Future Challenges. *Science* **2021**, *373*, eaaz8541.
- (8) Kim, T.; Shin, D.; Kim, M.; Kim, H.; Cho, E.; Choi, M.; Kim, J.; Jang, E.; Jeong, S. Development of Group III-V Colloidal Quantum Dots for Optoelectronic Applications. *ACS Energy Lett.* **2023**, *8*, 447–456.
- (9) Wang, H.; Li, Z.; Li, D.; Chen, P.; Pi, L.; Zhou, X.; Zhai, T. Van der Waals Integration Based on Two-Dimensional Materials for High-Performance Infrared Photodetectors. *Adv. Funct. Mater.* **2021**, *31*, 2103106.
- (10) Bergren, M. R.; Makarov, N. S.; Ramasamy, K.; Jackson, A.; Guglielmetti, R.; McDaniel, H. High-Performance CuInS<sub>2</sub> Quantum Dot Laminated Glass Luminescent Solar Concentrators for Windows. *ACS Energy Lett.* **2018**, *3*, 520–525.
- (11) Elbanna, A.; Jiang, H.; Fu, Q.; Zhu, J.-F.; Liu, Y.; Zhao, M.; Liu, D.; Lai, S.; Chua, X. W.; Pan, J.; Shen, Z. X.; Wu, L.; Liu, Z.; Qiu, C.-W.; Teng, J. 2D Material Infrared Photonics and Plasmonics. *ACS Nano* **2023**, *17*, 4134–4179.
- (12) Almutlaq, J.; Liu, Y.; Mir, W. J.; Sabatini, R. P.; Englund, D.; Bakr, O. M.; Sargent, E. H. Engineering Colloidal Semiconductor Nanocrystals for Quantum Information Processing. *Nat. Nanotechnol.* **2024**, *19*, 1091–1100.
- (13) Sandroni, M.; Wegner, K. D.; Aldakov, D.; Reiss, P. Prospects of Chalcopyrite-Type Nanocrystals for Energy Applications. *ACS Energy Letters* **2017**, *2*, 1076–1088.
- (14) Li, Y.; Min, J.; Jiang, Y.; Dong, T.; Xu, D.; Feng, Z.; Yan, Y.; Garoufalidis, C. S.; Baskoutas, S.; Shen, H.; Zeng, Z. Rational Design of Tetrahedral Derivatives as Efficient Light-Emitting Materials Based on “Super Atom” Perspective. *Nano Letters* **2024**, *24*, 3237–3242.
- (15) Park, H.; Kim, Y. S.; Hyun, S. C.; Kim, C. D.; Jin, M. S.; Kim, D. T.; Jang, K.; Kim, H. G.; Kim, W. T. Anomalous Dependence of Photoluminescence Properties on Composition x in Cd<sub>1-x</sub>Mn<sub>x</sub>Ga<sub>2</sub>S<sub>4</sub> Mixed Crystals. *Phys. Stat. Sol. b* **2006**, *3*, 2915–2918.
- (16) Radautsan, S. I.; Tiginyanu, I. M. Defect Engineering in II-III<sub>2</sub>-VI<sub>4</sub> and Related Compounds. *Jpn. J. Appl. Phys.* **1993**, *32*, 5–9.
- (17) Biswas, T.; Singh, A. K. Excitonic Effects in Absorption Spectra of Carbon Dioxide Reduction Photocatalysts. *Npj Comput. Mater.* **2021**, *7*, 189.
- (18) Singh, A. K.; Gorelik, R.; Biswas, T. Data-Driven Discovery of Robust Materials for Photocatalytic Energy Conversion. *Annu. Rev. Condens. Matter Phys.* **2023**, *14*, 237–259.
- (19) Mamedova, I. A.; Jahangirli, Z. A.; Kerimova, T. G.; Abdullayev, N. A. Bulk Modulus, Elastic Constants, and Force Constants of Interatomic Bonds of II-III<sub>2</sub>-VI<sub>4</sub> Compounds. *Phys. Stat. Sol. b* **2023**, *260*, 2200441.
- (20) Yeh, C.-Y.; Lu, Z. W.; Froyen, S.; Zunger, A. Zinc-Blende-Wurtzite Polytypism in Semiconductors. *Phys. Rev. B: Condens. Matter Mater. Phys.* **1992**, *46*, 10086–10097.
- (21) Jiang, X. S.; Yan, Y. C.; Yuan, S. M.; Mi, S.; Niu, Z. G.; Liang, J. Q. Trends in the Band-Gap Pressure Coefficients and Bulk Moduli in Different Structures of ZnGa<sub>2</sub>S<sub>4</sub>, ZnGa<sub>2</sub>Se<sub>4</sub> and ZnGa<sub>2</sub>Te<sub>4</sub>. *Chin. Phys. B* **2010**, *19*, 107104.
- (22) Joshi, N. V.; Luengo, J.; Vera, F. Optical Activity in ZnGa<sub>2</sub>S<sub>4</sub>. *Mater. Lett.* **2007**, *61*, 1926–1928.
- (23) Asadullayeva, S. G.; Jahangirli, Z. A.; Naghiyev, T. G.; Mammadov, D. A. Optical and Dynamic Properties of ZnGa<sub>2</sub>S<sub>4</sub>. *Phys. Status Solidi (b)* **2021**, *258*, 2100101.

- (24) Vilaplana, R.; Gomis, O.; Pérez-González, E.; Ortiz, H. M.; Manjón, F. J.; Rodríguez-Hernández, P.; Muñoz, A.; Alonso-Gutiérrez, P.; Sanjuán, M. L.; Ursaki, V. V.; Tiginyanu, I. M. Thermally Activated Cation Ordering in  $ZnGa_2Se_4$  Single Crystals Studied by Raman Scattering, Optical Absorption, and *Ab Initio* Calculations. *J. Phys: Condens. Matter* **2013**, *25*, 165802.
- (25) Babu, P.; Reddy, M. R. V.; Reddy, K. T. R. Photoluminescence Study of Chemical Bath Deposited  $ZnIn_2Se_4$  Thin Films. *Electron. Mater. Lett.* **2014**, *10*, 731–736.
- (26) Sheng, M.; Gan, C.; Li, Y.; Hu, Z.; Zhang, Y.; Gao, X.; Wang, X.; Jiang, H. Photocatalytic Degradable Polymer Precursor Production and C–C Bond Synthesis with  $CO_2$  over Sulfur Vacancies Enriched  $ZnIn_2S_4$  Nanosheets. *Chem. Eng. J.* **2022**, *446*, 136919.
- (27) Imran, M.; Ashraf, W.; Hafiz, A. K.; Khanuja, M. Synthesis and Performance Analysis of Photocatalytic Activity of  $ZnIn_2S_4$  Microspheres Synthesized Using a Low-Temperature Method. *ACS Omega* **2022**, *7*, 22987–22996.
- (28) Wu, T.; Bu, X.; Zhao, X.; Khazhakyan, R.; Feng, P. Phase Selection and Site-Selective Distribution by Tin and Sulfur in Supertetrahedral Zinc Gallium Selenides. *J. Am. Chem. Soc.* **2011**, *133*, 9616–9625.
- (29) Yadav, A. N.; Singh, K. Investigation of Photophysical Properties of Ternary Zn–Ga–S Quantum Dots: Band Gap versus Sub-Band-Gap Excitations and Emissions. *ACS Omega* **2019**, *4*, 18327–18333.
- (30) Lu, H.; Hu, Z.; Liu, H.; Fu, Z.; Dai, H.; Zhang, W.; Guo, R. Single-Phase Cu, Mn-Codoped  $ZnGaS/ZnS$  Quantum Dots for Full-Spectrum White-Light-Emitting Diodes. *ACS App. Nano Mater.* **2023**, *6*, 7375–7383.
- (31) Batabyal, S. K.; Lu, S. E.; Vittal, J. J. Synthesis, Characterization, and Photocatalytic Properties of  $In_2S_3$ ,  $ZnIn_2S_4$ , and  $CdIn_2S_4$  Nanocrystals. *Cryst. Growth Des.* **2016**, *16*, 2231–2238.
- (32) Rosales, B. A.; White, M. A.; Vela, J. Solution-Grown Sodium Bismuth Dichalcogenides: Toward Earth-Abundant, Biocompatible Semiconductors. *J. Am. Chem. Soc.* **2018**, *140*, 3736–3742.
- (33) Tappan, B. A.; Horton, M. K.; Brutcher, R. L. Ligand-Mediated Phase Control in Colloidal  $AgInSe_2$  Nanocrystals. *Chem. Mater.* **2020**, *32*, 2935–2945.
- (34) White, M. A.; Baumler, K. J.; Chen, Y.; Venkatesh, A.; Medina-Gonzalez, A. M.; Rossini, A. J.; Zaikina, J. V.; Chan, E. M.; Vela, J. Expanding the I–II–V Phase Space: Soft Synthesis of Polypyritic Ternary and Binary Zinc Antimonides. *Chem. Mater.* **2018**, *30*, 6173–6182.
- (35) Wegner, K. D.; Pouget, S.; Ling, W. L.; Carrière, M.; Reiss, P. Gallium – A Versatile Element for Tuning the Photoluminescence Properties of InP Quantum Dots. *Chem. Commun.* **2019**, *55*, 1663–1666.
- (36) Guo, Y.; Alvarado, S. R.; Barclay, J. D.; Vela, J. Shape-Programmed Nanofabrication: Understanding the Reactivity of Dichalcogenide Precursors. *ACS Nano* **2013**, *7*, 3616–3626.
- (37) Koziel, A. C.; Goldfarb, R. B.; Endres, E. J.; Macdonald, J. E. Molecular Decomposition Routes of Diaryl Diselenide Precursors in Relation to the Phase Determination of Copper Selenides. *Inorg. Chem.* **2022**, *61*, 14673–14683.
- (38) Brutcher, R. L. Diorganyl Dichalcogenides as Useful Synthons for Colloidal Semiconductor Nanocrystals. *Acc. Chem. Res.* **2015**, *48*, 2918–2926.
- (39) Yeung, M.; Popple, D. C.; Schriber, E. A.; Teat, S. J.; Beavers, C. M.; Demessence, A.; Kuykendall, T. R.; Hohman, J. N. Corrosion of Late- and Post-Transition Metals into Metal–Organic Chalcogenolates and Implications for Nanodevice Architectures. *ACS Appl. Nano Mater.* **2020**, *3*, 3568–3577.
- (40) Paritmongkol, W.; Lee, W. S.; Shcherbakov-Wu, W.; Ha, S. K.; Sakurada, T.; Oh, S. J.; Tisdale, W. A. Morphological Control of 2D Hybrid Organic–Inorganic Semiconductor AgSePh. *ACS Nano* **2022**, *16*, 2054–2065.
- (41) Mauritz, V.; Crisp, R. W. Unravelling the Intricacies of Solvents and Sulfur Sources in Colloidal Synthesis of Metal Sulfide Semiconductor Nanocrystals. *J. Mater. Chem. C* **2024**, *12*, 11319.
- (42) Kruszynska, M.; Borchert, H.; Parisi, J.; Kolny-Olesiak, J. Synthesis and Shape Control of  $CuInS_2$  Nanoparticles. *J. Am. Chem. Soc.* **2010**, *132*, 15976–15986.
- (43) Berto, F.; Haghigian, N.; Ferfolja, K.; Gardonio, S.; Fanetti, M.; Martelli, F.; Mussi, V.; Dubrovskii, V. G.; Shtrom, I. V.; Franciosi, A.; Rubini, S.  $Ga_2Se_3$  Nanowires via Au-Assisted Heterovalent Exchange Reaction on GaAs. *J. Phys. Chem. C* **2020**, *124*, 17783–17794.
- (44) Ho, C.-H.  $Ga_2Se_3$  Defect Semiconductors: The Study of Direct Band Edge and Optical Properties. *ACS Omega* **2020**, *5*, 18527–18534.
- (45) Yesinowski, J. P. Solid-State NMR of Inorganic Semiconductors. *Top. Curr. Chem.* **2011**, *306*, 229–312.
- (46) Larsen, F. H.; Jakobsen, H. J.; Ellis, P. D.; Nielsen, N. C. QCPMG-MAS NMR of Half-Integer Quadrupolar Nuclei. *J. Magn. Reson.* **1998**, *131*, 144–147.
- (47) Trebosc, J.; Wiench, J. W.; Huh, S.; Lin, V. S. Y.; Pruski, M. Studies of Organically Functionalized Mesoporous Silicas Using Heteronuclear Solid-State Correlation NMR Spectroscopy under Fast Magic Angle Spinning. *J. Am. Chem. Soc.* **2005**, *127*, 7587–7593.
- (48) Wiench, J.; Lin, V.-Y.; Pruski, M.  $^{29}Si$  NMR in Solid State with CPMG Acquisition under MAS. *J. Magn. Reson.* **2008**, *193*, 233–242.
- (49) Thayer, A. M.; Steigerwald, M. L.; Duncan, T. M.; Douglass, D. C. NMR Study of Semiconductor Molecular Clusters. *Phys. Rev. Lett.* **1988**, *60*, 2673–2676.
- (50) Tomaselli, M.; Yarger, J.; Bruchez, M., Jr.; Havlin, R.; DeGraw, D.; Pines, A.; Alivisatos, A. NMR Study of InP Quantum Dots: Surface Structure and Size Effects. *J. Chem. Phys.* **1999**, *110*, 8861–8864.
- (51) Cadars, S.; Smith, B.; Epping, J.; Acharya, S.; Belman, N.; Golani, Y.; Chmelka, B. Atomic Positional versus Electronic Order in Semiconducting ZnSe Nanoparticles. *Phys. Rev. Lett.* **2009**, *103*, 136802.
- (52) Nagashima, H.; Trébosc, J.; Calvez, L.; Pourpoint, F.; Mear, F.; Lafon, O.; Amoureux, J. P.  $^{71}Ga$ – $^{77}Se$  Connectivities and Proximities in Gallium Selenide Crystal and Glass Probed by Solid-State NMR. *J. Magn. Reson.* **2017**, *282*, 71–82.
- (53) Woods-Robinson, R.; Han, Y.; Zhang, H.; Ablekim, T.; Khan, I.; Persson, K. A.; Zakutayev, A. Wide Band Gap Chalcogenide Semiconductors. *Chem. Rev.* **2020**, *120*, 4007–4055.
- (54) Owen, J. The Coordination Chemistry of Nanocrystal Surfaces. *Science* **2015**, *347*, 615–616.
- (55) Biesterfeld, L.; Klepzig, L. F.; Niebur, A.; Rosebrock, M.; Lauth, J. Toward Bright Colloidal Near-Infrared Emitters: Surface Passivation of 2D PbSe Nanoplatelets by Metal Halides. *J. Phys. Chem. C* **2022**, *126*, 19277–19285.
- (56) Jung, B. K.; Yoo, H.; Seo, B.; Choi, H. J.; Choi, Y. K.; Kim, T. H.; Oh, N.; Kim, S. Y.; Kim, S.; Lee, Y.; Shim, J. W.; Park, H. Y.; Hwang, G. W.; Ng, T. N.; Oh, S. J. High-Affinity Ligand-Enhanced Passivation of Group III–V Colloidal Quantum Dots for Sensitive Near-Infrared Photodetection. *ACS Energy Letters* **2024**, *9*, 504–512.
- (57) Kirkwood, N.; Monchen, J. O. V.; Crisp, R. W.; Grimaldi, G.; Bergstein, H. A. C.; Du Fossé, I.; van der Stam, W.; Infante, I.; Houtepen, A. J. Finding and Fixing Traps in II–VI and III–V Colloidal Quantum Dots: The Importance of Z-Type Ligand Passivation. *J. Am. Chem. Soc.* **2018**, *140*, 15712–15723.
- (58) Eagle, F. W.; Park, N.; Cash, M.; Cossairt, B. M. Surface Chemistry and Quantum Dot Luminescence: Shell Growth, Atomistic Modification, and Beyond. *ACS Energy Lett.* **2021**, *6*, 977–984.
- (59) Mohebpour, M. A.; Mortazavi, B.; Rabczuk, T.; Zhuang, X.; Shapeev, A. V.; Tagani, M. B. Mechanical, Optical, and Thermoelectric Properties of Semiconducting  $ZnIn_2X_4$  ( $X = S, Se, Te$ ) Monolayers. *Phys. Rev. B* **2022**, *105*, 134108.
- (60) Miller, G. J. The “Coloring Problem” in Solids: How It Affects Structure, Composition and Properties. *Eur. J. Inorg. Chem.* **1998**, *1998*, 523–536.
- (61) Schnepf, R. R.; Cordell, J. J.; Tellekamp, M. B.; Melamed, C. L.; Greenaway, A. L.; Mis, A.; Brennecka, G. L.; Christensen, S.; Tucker, G. J.; Toberer, E. S.; Lany, S.; Tamboli, A. C. Utilizing Site Disorder

in the Development of New Energy-Relevant Semiconductors. *ACS Energy Lett.* **2020**, *5*, 2027–2041.

(62) Kresse, G.; Furthmüller, J. Efficient Iterative Schemes for *Ab Initio* Total-Energy Calculations Using a Plane-Wave Basis Set. *Phys. Rev. B: Condens. Matter Mater. Phys.* **1996**, *54*, 11169–11186.

(63) Haynes, W. M. Atomic Radii of the Elements. In *CRC Handbook of Chemistry and Physics*; CRC Press: Boca Raton, FL, 2016. pp 9–49–9–50.

(64) Chandler, D.; Weeks, J. D.; Andersen, H. C. Van Der Waals Picture of Liquids, Solids, and Phase Transformations. *Science* **1983**, *220*, 787–794.

(65) Andersen, O. K. Linear Methods in Band Theory. *Phys. Rev. B* **1975**, *12*, 3060.